

Exploring State Space Model in Wavelet Domain: An Infrared and Visible Image Fusion Network via Wavelet Transform and State Space Model

Tianpei Zhang^{1,†}, Yiming Zhu^{1,†}, Jufeng Zhao^{1,✉}, Guangmang Cui¹, Yuchen Zheng¹

¹*School of Electronics and Information Engineering, Hangzhou Dianzi University, Hangzhou, China*
232040138@hdu.edu.cn, yiming_zhu_hdu@163.com, dabaozjf@hdu.edu.cn,
cuigm@hdu.edu.cn, 232040254@hdu.edu.cn

Abstract—Deep learning techniques have revolutionized the infrared and visible image fusion (IVIF), showing remarkable efficacy on complex scenarios. However, current methods do not fully combine frequency domain features with global semantic information, which will result in suboptimal extraction of global features across modalities and insufficient preservation of local texture details. To address these issues, we propose Wavelet-Mamba (W-Mamba), which integrates wavelet transform with the state-space model (SSM). Specifically, we introduce Wavelet-SSM module, which incorporates wavelet-based frequency domain feature extraction and global information extraction through SSM, thereby effectively capturing both global and local features. Additionally, we propose a cross-modal feature attention modulation, which facilitates efficient interaction and fusion between different modalities. The experimental results indicate that our method achieves both visually compelling results and superior performance compared to current state-of-the-art methods. Our code is available at <https://github.com/Lmmh058/W-Mamba>.

Index Terms—wavelet transform, state-space model, image fusion, cross-modal feature modulation.

I. INTRODUCTION

Infrared and visible light images exhibit strong complementary characteristics. Specifically, visible images have rich texture details but are sensitive to lighting variations, while infrared images provide thermal information but lack texture details. Therefore, IVIF can effectively integrate the information of visible and infrared images with rich textures and prominent targets, which is not only enhances human visual observation, but also significantly improves advanced computer vision tasks, such as object detection [1], [2], semantic segmentation [3], and tracking [4].

Currently, IVIF methods mainly rely on convolutional neural networks, including U2Fusion [5] and DenseFuse [6]. These methods combine both image-level and feature-level features, but overlook long-range dependencies during feature extraction, which can decrease fusion performance. GAN-based methods, such as GANMcC [7], transform image fusion as an adversarial learning problem, emphasizing global information, but neglecting the interaction of different domains feature. The vision Transformer based method, such as DATFuse

[8], utilize self-attention to capture long-range dependencies. However, computation of self-attention mechanisms faces the challenge of quadratic complexity. State-space models (SSMs) have emerged as competitive methods, offering linear scalability to capture long-range dependency. Recently, the Mamba framework [9], such as FusionMamba [10], have exhibited outstanding performance in image fusion by capitalizing on the linear complexity of SSM and its exceptional visual modeling capabilities.

In addition to effective long-range dependency modeling, we argue that the key bottleneck of IVIF lies in comprehensive feature extraction across spatial and frequency domains. Recently, the frequency domain fusion method [11] achieved promising results by extracting frequency information. However, CNN-based methods [12] typically focus on high-frequency features while neglecting low-frequency information, while SSM and Transformer excel in capturing long-range dependencies but face challenges in preserving high-frequency features such as edges and textures. Therefore, how to separate high- and low-frequency information and the interaction of frequency-spatial features is remains a problem worth considering. Therefore, IVIF must not only prioritize the global receptive field for feature extraction but also fully integrate the frequency domain features and the information interaction between modalities.

To address the aforementioned problem, we propose Wavelet-Mamba (W-Mamba), which first utilize wavelet transform decomposes image features into low-frequency components that capture structural information and high-frequency sub-bands that contain texture details. Additionally, We combine the advantages of SSM in modeling long-range dependence with the ability of wavelet transform in frequency feature extraction. A cross-domain attention feature modulation was designed to explore intra-inter modal features. This integration enhances feature perception and cross-modal feature interaction in IVIF, improving overall performance. The contributions of this work are as follows:

- We propose a novel IVIF framework that comprehensively extracts frequency-domain features, effectively complementing spatial-domain features.
- We designed the Wavelet-SSM Feature Extraction module, which extracts both global features and local details

[†] Equal Contribution. [✉] Corresponding author. This research was supported by the Zhejiang Provincial Natural Science Foundation of China (Grant No. LY22F050002) and the Graduate Scientific Research Foundation of Hangzhou Dianzi University (Grant No. CXJJ2024070).

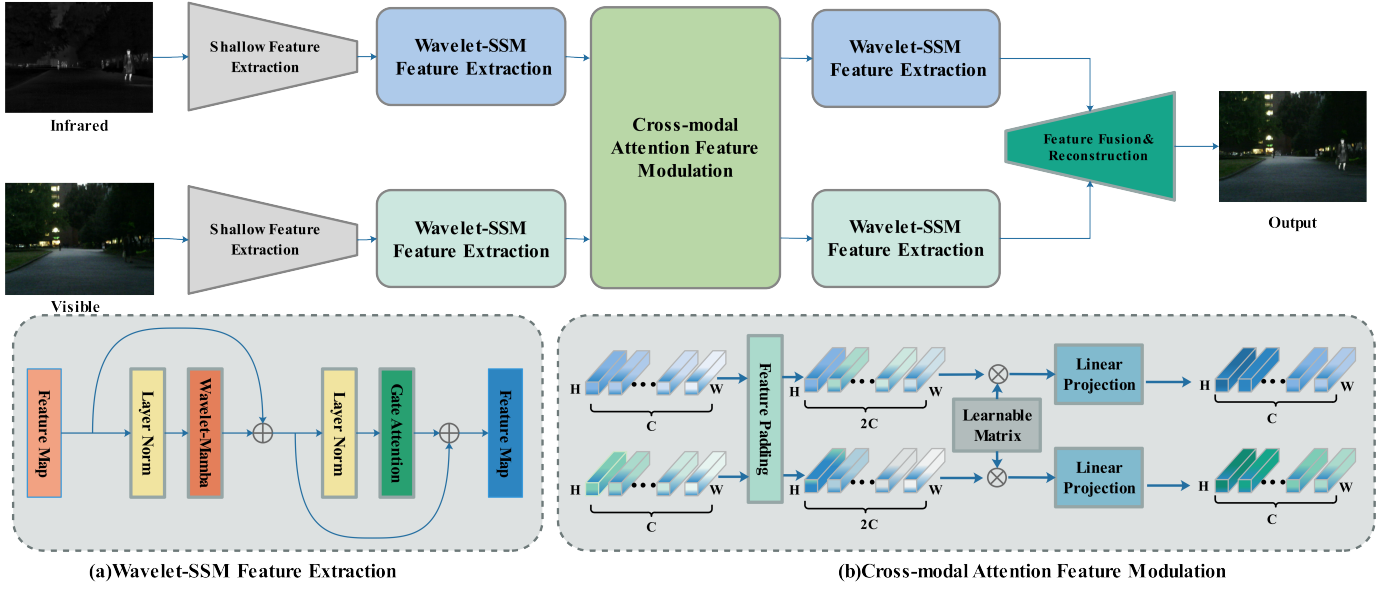


Fig. 1. The overall structure of the proposed W-Mamba, highlighting the core components of the W-Mamba module. This architecture features two uniquely designed modules: the Wavelet-SSM Feature Extraction (WFE) (a) and the Cross-modal Attention Feature Modulation (CAFM) (b).

from the frequency domain.

- We designed a cross-modal feature modulation module that facilitates the efficient interaction of complementary features by fully learning their interdependencies.

II. METHOD

A. Overall Framework

The architecture of Wavelet-Mamba (W-Mamba) is depicted in Fig. 1. Initially, the source images I^{vi} and I^{ir} , with dimensions $R^{C \times H \times W}$, are inputted separately into a CNN-based shallow feature extraction module to extract more informative feature representations.

$$f_{sf}^{vi} = SF(I^{vi}), f_{sf}^{ir} = SF(I^{ir}) \quad (1)$$

where f_{sf}^{vi} and $f_{sf}^{ir} \in R^{C' \times H' \times W'}$ ($H' = \frac{H}{2}, W' = \frac{W}{2}$) represent the shallow features extracted by the shallow feature extraction module $SF(\cdot)$. The source images are downsampled to reduce computational complexity, and their channels are mapped to C' to enhance the capacity for feature representation. Subsequently, the Wavelet-SSM Feature Extraction Network (WFE) efficiently captures comprehensive frequency-domain information.

$$f_{df}^{vi} = WFE(f_{sf}^{vi}), f_{df}^{ir} = WFE(f_{sf}^{ir}) \quad (2)$$

where f_{df}^{vi} and f_{df}^{ir} represent the deep features extracted by $WFE(\cdot)$. The network then performs Cross-Modal Attention Feature Modulation (CAFM) to enhance feature interactions and utilize complementary information, thereby reinforcing the original modality features through an additional WFE.

$$\begin{aligned} f_{ccf}^{vi} &= WFE(CAFM(f_{df}^{vi})) \\ f_{ccf}^{ir} &= WFE(CAFM(f_{df}^{ir})) \end{aligned} \quad (3)$$

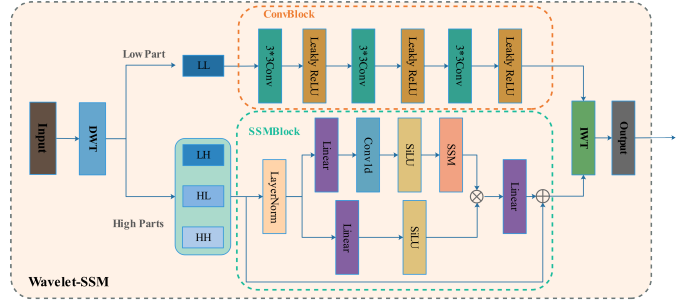


Fig. 2. The detailed structure of the Wavelet-Mamba in Fig.1(a).

where f_{ccf}^{vi} and f_{ccf}^{ir} represent the comprehensive cross-modal features. Finally, f_{ccf}^{vi} and f_{ccf}^{ir} are passed through a CNN-based fusion and reconstruction module with upsampling to integrate the features and map them back to the original image space.

$$I_F = F\&R(f_{ccf}^{vi}, f_{ccf}^{ir}) \quad (4)$$

where $F\&R(\cdot)$ denotes the feature fusion and reconstruction module, and I_F represents the fused image.

B. Wavelet-SSM Feature Extraction

1) **State Space Model:** The State Space Model (SSM) [10] maps the input sequence $x(t)$ to a latent state representation $h'(t)$ using state equations and generates the predicted output $y(t)$ through output equations:

$$h'(t) = Ah(t) + Bx(t), y(t) = Ch(t) + Dx(t) \quad (5)$$

where $h'(t)$ represents the current state, $h(t)$ denotes the previous state, and $A, B, C,$ and D are the model parameters. To integrate the SSM into deep learning, the Zero-Order

Hold (ZOH) technique is utilized for discretization. Vision Mamba replaces the traditional self-attention mechanism with a bidirectional SSM, leveraging it to model sequential data and efficiently capture long-range dependencies.

2) **Architecture:** The structure of WFE is shown in Fig.1(a), and the process is described as follows:

$$\begin{aligned} f' &= f + WM(LN(f)) \\ f_{out} &= f' + GAM(LN(f')) \end{aligned} \quad (6)$$

where f represents the input to the WFE, $LN(\cdot)$ denotes the layer normalization operation, $WM(\cdot)$ represents the Wavelet-Mamba operation, $GAM(\cdot)$ denotes the gated attention mechanism, and f_{out} is the output of the WFE.

Wavelet-Mamba: The detailed structure of the Wavelet-Mamba is illustrated in Fig.2. A two-dimensional discrete wavelet transform (2D-DWT) is applied to the input features, decomposing them into low-frequency and high-frequency components:

$$LL, LH, HL, HH = 2DDWT(f_{WM}^{in}) \quad (7)$$

where, f_{WM}^{in} represents the input to the Wavelet-Mamba block. The LL component corresponds to low-frequency features, while LH , HL , and HH represent high-frequency components. Low-frequency features are processed using convolutional layers, whereas high-frequency features are refined via SSM to capture long-range dependencies. This approach facilitates the comprehensive extraction of global features and local details in the frequency domain. Finally, an inverse transformation reconstructs these features back into the spatial domain.

$$\begin{aligned} f_{lf} &= ConvBlock(LL) \\ f_{hf} &= SSMBlock(\{LH, HL, HH\}) \\ f_{WM}^{out} &= 2DIWT(concat(f_{lf}, f_{hf})) \end{aligned} \quad (8)$$

where f_{lf} and f_{hf} represent the feature maps produced by the convolution operations $ConvBlock(\cdot)$ and the SSM process $SSMBlock(\cdot)$, respectively. The final output vector f_{WM}^{out} is obtained by concatenating ($concat(\cdot)$) these feature maps, followed by the inverse wavelet transformation $2DIWT(\cdot)$.

Gated Attention Mechanism: Inspired by [13], we propose a gated mechanism utilizing depthwise separable convolutions (Fig.3) for dynamic information control. Depthwise convolutions capture weights based on local relationships, facilitating efficient feature extraction while minimizing redundancy and reducing parameter overhead.

$$\begin{aligned} f_{att}, w_{att} &= Split(Conv_1^{C, 2C}(LN(f_{GAM}^{in}))) \\ f_{GAM}^{out} &= f_{GAM}^{in} + PWConv(f_{att} \otimes DWConv(w_{att})) \end{aligned} \quad (9)$$

where, f_{GAM}^{in} represents the input, $Conv_1^{C, 2C}(\cdot)$ denotes a 1×1 convolution that maps C channels to $2C$ channels, and $Split(\cdot)$ performs channel-wise splitting to produce the feature f_{att} and the weight w_{att} . The symbol \otimes represents element-wise multiplication, while $DWConv(\cdot)$ and $PWConv(\cdot)$ denote depth-wise and point-wise convolutions, respectively. The output of the GAM module is f_{GAM}^{out} .

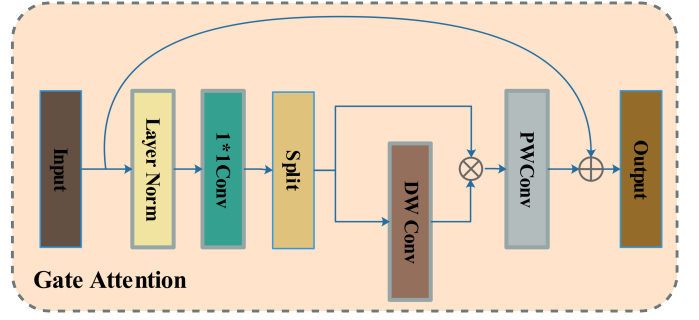


Fig. 3. The detailed structure of the Gated Attention in Fig.1(a).

C. Cross-modal Attention Feature Modulation

The Cross-modal Attention Feature Modulation (CAFM) is shown in Fig.1(b). It enhances single-modal features by leveraging cross-modal complementary information, thereby improving feature expressiveness while preserving the original information. For the inputs $f_{vi}^{in}, f_{ir}^{in} \in R^{C' \times H' \times W'}$, the padding process is defined as:

$$\begin{aligned} f_{vi}^{pf} &= [f_{vi}^1, f_{ir}^1, f_{vi}^2, f_{ir}^2, \dots, f_{vi}^n, f_{ir}^n] \\ f_{ir}^{pf} &= [f_{ir}^1, f_{vi}^1, f_{ir}^2, f_{vi}^2, \dots, f_{ir}^n, f_{vi}^n] \end{aligned} \quad (10)$$

where $f_{vi}^i, f_{ir}^i \in R^{1 \times H' \times W'}$ are the i -th channels of f_{vi}^{in} and f_{ir}^{in} , while $f_{vi}^{pf}, f_{ir}^{pf} \in R^{2C' \times H' \times W'}$ are the padded features. Meanwhile, a learnable weight matrix and linear projection map the padded features for modality enhancement and adjustment of dimensions.

$$\begin{aligned} f_{vi}^{out} &= Proj_{2C'}^{C'}(\mathcal{I}^{vi} \otimes f_{vi}^{pf}) \\ f_{ir}^{out} &= Proj_{2C'}^{C'}(\mathcal{I}^{ir} \otimes f_{ir}^{pf}) \end{aligned} \quad (11)$$

where $\mathcal{I}^{vi}, \mathcal{I}^{ir} \in R^{2C' \times 1 \times 1}$ represent the weights parameters, and $Proj_{2C'}^{C'}(\cdot)$ denotes a linear projection reducing $2C'$ channels to C' . This process yields f_{vi}^{out} and f_{ir}^{out} , embedding original modality and cross-domain complement.

D. Loss function

We train W-Mamba by intensity and gradient loss to preserve structural textures and regulate intensity. The overall loss function is defined as:

$$\mathcal{L}_{all} = \lambda_1 \mathcal{L}_{int} + \lambda_2 \mathcal{L}_{grad} \quad (12)$$

where λ_1 and λ_2 are weighting parameters used to balance the two sub-loss functions. The intensity loss encourages the training network to preserve more meaningful pixel intensity information. \mathcal{L}_{int} is defined as shown in Eq. 13.

$$\mathcal{L}_{int} = \frac{1}{HW} \|I_F - \max(I^{ir}, I^{vi})\|_1 \quad (13)$$

in Eq. 13, $\max(\cdot)$ denotes the element-wise maximum operation. Additionally, The gradient loss is designed to retain as much texture detail as possible from both modalities. \mathcal{L}_{grad} is defined in Eq. 14.

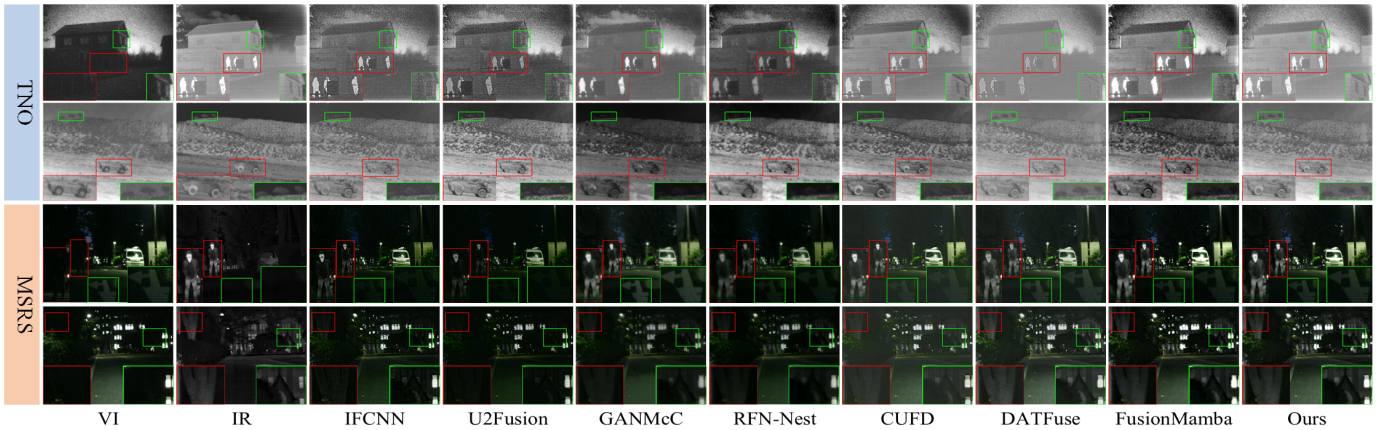


Fig. 4. Qualitative comparison of W-Mamba and seven comparative methods on TNO (top two rows) and MSRS (bottom two rows) dataset. We highlight two key regions in the image with red and green bounding boxes, respectively, and magnify them to simplify the visual comparison process.

$$\mathcal{L}_{grad} = \frac{1}{HW} \|\|\nabla I_F - \max(|\nabla I^{ir}|, |\nabla I^{vi}|)\|\|_1 \quad (14)$$

where ∇ is Sobel gradient operator, $\max(\cdot)$ denotes the element-wise maximum selection.

III. EXPERIMENT RESULTS AND ANALYSIS

A. Experiment Configurations

Implementation details: We randomly cropped pairs of image patches with dimensions 128×128 from the TNO [14], MSRS [15] and LLVIP [16] datasets, and normalizing their pixel intensity to the range $[0, 1]$. The Adam optimizer was employed with a learning rate of 2.5×10^{-5} . The batch size was set to 24. The hyperparameters of the loss function, λ_1 and λ_2 were empirically set to 10 and 1, respectively. All experiments were conducted on a NVIDIA GeForce RTX 4090D GPU. Finally, we evaluate W-Mamba on the TNO [14] and MSRS [15] datasets to assess the performance.

Evaluation metrics: We selected AE-based methods RFN-Nest [17] and CUFD [18], CNN-based methods U2Fusion [5] and IFCNN [19], GAN-based method GANMcC [7], Transformer-based method DATFuse [8], and Mamba-based method FusionMamba [10]. Additionally, we employed six widely recognized metrics for quantitative evaluation, including two information-theory-based metrics: mutual information (MI) [20] and nonlinear correlation information entropy (NCIE) [21]; two image feature-based metrics: gradient-based similarity measurement (Q_{abf}) [22] and phase congruency (Q_p) [23]; one structural similarity-based metric: Yang’s metric (Q_y) [24]; and one human visual perception-based metric: visual information fidelity (VIF) [25].

B. Experiment results

Quantitative Analysis: The quantitative results are presented in Tab.I and Fig.5. Our approach consistently outperforms the others on six evaluation metrics. The results demonstrate that W-Mamba effectively extracts complementary information from source images, producing fused images

TABLE I

QUANTITATIVE COMPARISONS BETWEEN W-MAMBA AND SEVEN METHODS ON THE TNO [14] AND MSRS [15] DATASETS. THE TOP THREE PERFORMERS FOR EACH METRIC ARE HIGHLIGHTED IN RED, BLUE, AND GREEN, RESPECTIVELY. \uparrow INDICATES THAT HIGHER VALUES CORRESPOND TO BETTER PERFORMANCE.

	TNO	MI \uparrow	NCIE \uparrow	Q_{abf} \uparrow	Q_p \uparrow	Q_y \uparrow	VIF \uparrow
IFCNN [19]	1.4711	0.8048	0.4765	0.3060	0.7769	0.6370	
U2Fusion [5]	1.4338	0.8046	0.4254	0.2862	0.7276	0.6273	
GANMcC [7]	1.6432	0.8052	0.2884	0.2389	0.5978	0.5270	
RFN-Nest [17]	1.5059	0.8048	0.3375	0.2154	0.6267	0.5625	
CUFD [18]	2.3848	0.8086	0.3985	0.3014	0.7599	0.6668	
DATFuse [8]	2.2060	0.8077	0.5065	0.3786	0.8955	0.6966	
FusionMamba [10]	1.8387	0.8062	0.3374	0.2008	0.6301	0.5601	
*Ours	3.0997	0.8135	0.5492	0.4297	0.9083	0.8329	
	MSRS	MI \uparrow	NCIE \uparrow	Q_{abf} \uparrow	Q_p \uparrow	Q_y \uparrow	VIF \uparrow
IFCNN [19]	1.0252	0.8032	0.4550	0.2455	0.6287	0.6332	
U2Fusion [5]	1.0515	0.8035	0.3403	0.2169	0.5029	0.4968	
GANMcC [7]	1.4613	0.8044	0.3439	0.2476	0.6672	0.6730	
RFN-Nest [17]	1.3233	0.8042	0.3115	0.2574	0.5544	0.6037	
CUFD [18]	1.3803	0.8046	0.3906	0.2456	0.5741	0.5781	
DATFuse [8]	1.9270	0.8068	0.5608	0.3594	0.7705	0.8853	
FusionMamba [10]	1.5411	0.8050	0.4187	0.2228	0.6796	0.7417	
*Ours	2.4309	0.8100	0.6017	0.4335	0.8707	0.9626	

with enriched information, comprehensive features, and strong structural similarity.

Qualitative Analysis: The fusion results of W-Mamba and other methods on the TNO [14] and MSRS [15] are shown in Fig.4. IFCNN, U2Fusion, and FusionMamba in Fig.4 introduced considerable noise, such as the green box in the first row, which caused the loss of edge information. The green box in the second row indicates that our method has better fusion performance in two source images where the foreground and background brightness are opposite. In the infrared images with grayscale or RGB images fusion, DATFuse has low contrast in the grayscale fusion results, such as the window detail to the left of the green box in the first row of Fig.4. However, CUFD has low contrast in RGB image fusion, resulting in unclear visible and infrared edge information. Overall, W-Mamba can utilize complementary information from two modalities, can fusion results with clear

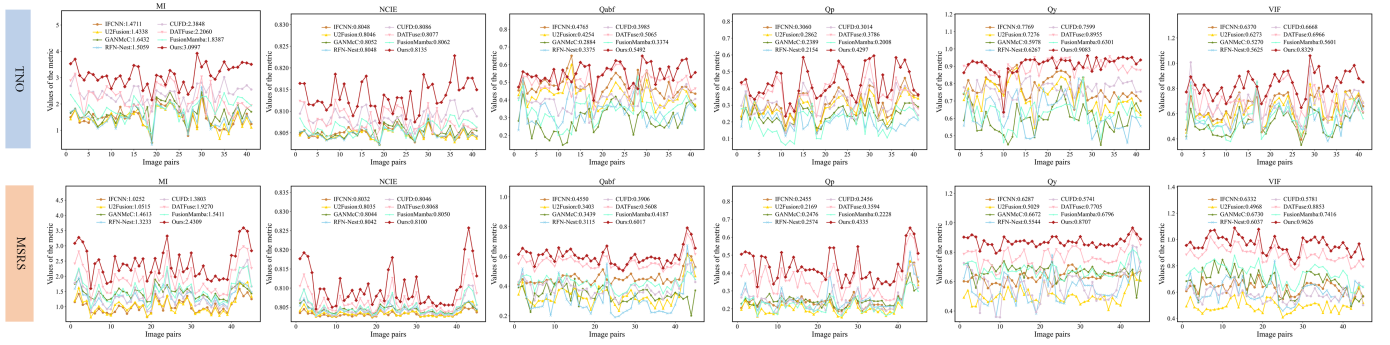


Fig. 5. Quantitative comparison of W-Mamba and seven comparison methods on TNO [14] and MSRS [15] dataset. Our method is represented by the red line. Mean values of each method are shown in each legend. For the 6 metrics used for comparison, a higher value indicates superior performance.

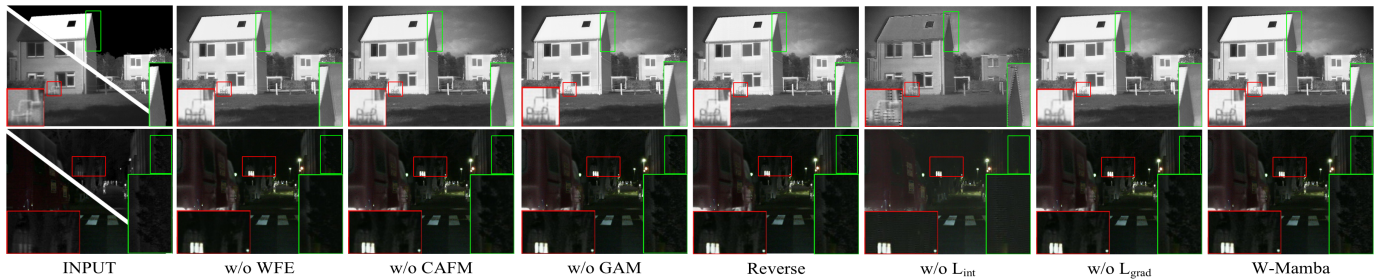


Fig. 6. Qualitative comparison of W-Mamba ablation experiment. We highlight two key regions in the image with red and green bounding boxes, respectively, and magnify them to simplify the visual comparison process.

TABLE II
QUANTITATIVE COMPARISON OF ABLATION EXPERIMENTS. **RED** REPRESENTS THE BEST RESULT. **REVERSE** REPRESENTS APPLYING SSM TO LOW-FREQUENCY PART. \uparrow INDICATES THAT HIGHER METRICS THE BETTER PERFORMANCE.

	MI \uparrow	NCIE \uparrow	$Q_{abf}\uparrow$	$Q_p\uparrow$	$Q_y\uparrow$	VIF \uparrow
w/o WFE	2.5857	0.8101	0.4685	0.3337	0.8129	0.6946
w/o CAFM	2.8825	0.8119	0.5096	0.3812	0.8795	0.7723
w/o GAM	3.0019	0.8128	0.5363	0.4158	0.9013	0.8138
Reverse	2.7409	0.8110	0.4932	0.3645	0.8619	0.7475
w/o L_{int}	1.3338	0.8047	0.4649	0.3171	0.4276	0.3478
w/o L_{grad}	2.6198	0.8102	0.4497	0.3281	0.8198	0.6838
*W-Mamba	3.0997	0.8135	0.5492	0.4297	0.9083	0.8329

edges, prominent targets, thus alignment well with visual perception.

C. Ablation Study

Quantitative Analysis: The ablation studies are conducted from two perspectives: **network architecture** ablation (w/o WFE, CAFM, GAM and reverse SSM frequency band) and **loss function** ablation (w/o L_{int} and L_{grad}). As shown in Tab.II. The remove of WFE, CAFM and GAM resulted in a decline in all six evaluation indicators, demonstrating the effectiveness of frequency domain information and global information, and demonstrating the importance of complementary information between modalities. Furthermore, when SSM is applied to low-frequency signals in wavelet transform, each indicator experiences a degradation, indicating that SSM can

better extract complementary features in high-frequency parts. Finally, the removal of the intensity loss function and gradient loss function, Q_{abf} and Q_p will significantly decrease, indicating that the gradient loss function is crucial in preserving details.

Qualitative Analysis: The qualitative results are presented in Fig.6, revealing the following observations: 1) After removing WFE, the feature extraction performance declines and resulting in significant performance degradation, which is artifacts in the green box of the first row. The intensity information is lost in the red box of the second row, resulting in blurred edges after fusion. 2) Removing CAFM presents challenges in enhancing complementary features, resulting in edge artifacts in the green box of the first row. 3) The removal of GAM partially reduces the ability to capture local relationships in the source images, leading to blurred leaf details in the green box of the second row. 4) When SSM is applied to the low-frequency components, the green box in the first row displays pseudo edges at the edge of the roof, indicating that SSM is effective in capturing long-range dependencies in the high-frequency. 5) After removing the intensity loss function, the fusion result fails to produce appropriate intensity, and some distortion occurs such as the red and green boxes in the first row. 6)After removing the gradient loss function, the edges of the fused image generated at the edge of the chair in the first row are blurred.

TABLE III

QUANTITATIVE COMPARISON OF OBJECT DETECTION ON THE MSRS [15] DATASET. THE BEST-PERFORMING METHOD IS HIGHLIGHTED IN RED. \uparrow INDICATES THAT HIGHER VALUES CORRESPOND TO BETTER PERFORMANCE.

Method	mAP@0.65 \uparrow	mAP@0.85 \uparrow	mAP@[0.5,0.95] \uparrow
IFCNN [19]	0.806	0.473	0.621
U2Fusion [5]	0.837	0.498	0.636
GANMcC [7]	0.842	0.534	0.656
RFN-Nest [17]	0.775	0.476	0.593
CUFD [18]	0.849	0.507	0.649
DATFuse [8]	0.843	0.497	0.645
FusionMamba [10]	0.797	0.497	0.622
*Ours	0.848	0.565	0.659

D. Downstream application

To demonstrate the superiority of W-Mamba in downstream tasks, we fused 80 pairs of labeled images from the MSRS dataset with YOLOv5. Tab.III presents the mean average precision (mAP) under various intersection over union (IoU) thresholds. The results indicate that our method achieves the highest performance in mAP@[0.5, 0.95], demonstrating its robust mAP performance. This further validates the effectiveness of W-Mamba.

IV. DISCUSSION AND CONCLUSION

In this paper, We propose Wavelet-Mamba (W-Mamba). The key innovation is Wavelet-SSM Feature Extraction module, which combines frequency domain information with SSM. We also propose a gated attention mechanism to extract details near the edges. Additionally, we propose cross-modal attention feature modulation, which dynamically fuses cross-modal features. The experimental results show that our method is superior to existing IVIF methods and enhances visual perception in the fused images.

REFERENCES

- [1] C. Hu, X. Dong, Y. H. L. Wang, L. Xu, T. Pu, and Z. Peng, "Smpisd-mtpnet: Scene semantic prior-assisted infrared ship detection using multi-task perception networks," *arXiv preprint arXiv:2407.18487*, 2024.
- [2] Y. Zhu, Y. Ma, F. Fan, J. Huang, K. Wu, and G. Wang, "Towards accurate infrared small target detection via edge-aware gated transformer," *IEEE Journal of Selected Topics in Applied Earth Observations and Remote Sensing*, 2024.
- [3] C. Hu, Y. Huang, K. Li, L. Zhang, Y. Zhu, Y. Peng, T. Pu, and Z. Peng, "Gradient is all you need: Gradient-based attention fusion for infrared small target detection," *arXiv preprint arXiv:2409.19599*, 2024.
- [4] A. Yilmaz, O. Javed, and M. Shah, "Object tracking: A survey," *Acm computing surveys (CSUR)*, vol. 38, no. 4, pp. 13–es, 2006.
- [5] H. Xu, J. Ma, J. Jiang, X. Guo, and H. Ling, "U2fusion: A unified unsupervised image fusion network," *IEEE Transactions on Pattern Analysis and Machine Intelligence*, vol. 44, no. 1, pp. 502–518, 2020.
- [6] H. Li and X.-J. Wu, "Densefuse: A fusion approach to infrared and visible images," *IEEE Transactions on Image Processing*, vol. 28, no. 5, pp. 2614–2623, 2018.
- [7] J. Ma, H. Zhang, Z. Shao, P. Liang, and H. Xu, "Ganmcc: A generative adversarial network with multiclassification constraints for infrared and visible image fusion," *IEEE Transactions on Instrumentation and Measurement*, vol. 70, pp. 1–14, 2020.
- [8] W. Tang, F. He, Y. Liu, Y. Duan, and T. Si, "Datfuse: Infrared and visible image fusion via dual attention transformer," *IEEE Transactions on Circuits and Systems for Video Technology*, vol. 33, no. 7, pp. 3159–3172, 2023.
- [9] A. Gu and T. Dao, "Mamba: Linear-time sequence modeling with selective state spaces," *arXiv preprint arXiv:2312.00752*, 2023.
- [10] X. Xie, Y. Cui, C.-I. Jeong, T. Tan, X. Zhang, X. Zheng, and Z. Yu, "Fusionmamba: Dynamic feature enhancement for multimodal image fusion with mamba," *arXiv preprint arXiv:2404.09498*, 2024.
- [11] G. Xiao, Z. Tang, H. Guo, J. Yu, and H. T. Shen, "Fafusion: Learning for infrared and visible image fusion via frequency awareness," *IEEE Transactions on Instrumentation and Measurement*, vol. 73, pp. 1–11, 2024.
- [12] C. Si, W. Yu, P. Zhou, Y. Zhou, X. Wang, and S. Yan, "Inception transformer," *Advances in Neural Information Processing Systems*, vol. 35, pp. 23 495–23 509, 2022.
- [13] Y. Wang, Y. Li, G. Wang, and X. Liu, "Multi-scale attention network for single image super-resolution," in *Proceedings of the IEEE/CVF Conference on Computer Vision and Pattern Recognition (CVPR) Workshops*, June 2024, pp. 5950–5960.
- [14] A. Toet, "The tno multiband image data collection," *Data in brief*, vol. 15, pp. 249–251, 2017.
- [15] L. Tang, J. Yuan, H. Zhang, X. Jiang, and J. Ma, "Piafusion: A progressive infrared and visible image fusion network based on illumination aware," *Information Fusion*, vol. 83, pp. 79–92, 2022.
- [16] X. Jia, C. Zhu, M. Li, W. Tang, and W. Zhou, "Llvip: A visible-infrared paired dataset for low-light vision," in *Proceedings of the IEEE/CVF international conference on computer vision*, 2021, pp. 3496–3504.
- [17] H. Li, X.-J. Wu, and J. Kittler, "Rfn-nest: An end-to-end residual fusion network for infrared and visible images," *Information Fusion*, vol. 73, pp. 72–86, 2021.
- [18] H. Xu, M. Gong, X. Tian, J. Huang, and J. Ma, "Cufd: An encoder-decoder network for visible and infrared image fusion based on common and unique feature decomposition," *Computer Vision and Image Understanding*, vol. 218, p. 103407, 2022.
- [19] Y. Zhang, Y. Liu, P. Sun, H. Yan, X. Zhao, and L. Zhang, "Ifcnn: A general image fusion framework based on convolutional neural network," *Information Fusion*, vol. 54, pp. 99–118, 2020.
- [20] G. Qu, D. Zhang, and P. Yan, "Information measure for performance of image fusion," *Electronics letters*, vol. 38, no. 7, p. 1, 2002.
- [21] Q. Wang, Y. Shen, and J. Q. Zhang, "A nonlinear correlation measure for multivariable data set," *Physica D: Nonlinear Phenomena*, vol. 200, no. 3–4, pp. 287–295, 2005.
- [22] C. S. Xydeas, V. Petrovic *et al.*, "Objective image fusion performance measure," *Electronics letters*, vol. 36, no. 4, pp. 308–309, 2000.
- [23] J. Zhao, R. Laganieri, and Z. Liu, "Performance assessment of combinative pixel-level image fusion based on an absolute feature measurement," *Int. J. Innov. Comput. Inf. Control*, vol. 3, no. 6, pp. 1433–1447, 2007.
- [24] S. Li, R. Hong, and X. Wu, "A novel similarity based quality metric for image fusion," in *2008 International Conference on Audio, Language and Image Processing*. IEEE, 2008, pp. 167–172.
- [25] Y. Han, Y. Cai, Y. Cao, and X. Xu, "A new image fusion performance metric based on visual information fidelity," *Information fusion*, vol. 14, no. 2, pp. 127–135, 2013.